

Targeting endothelial coagulation signaling ameliorates liver obstructive cholestasis and dysfunctional angiogenesis

Xue Yang^{1,2*}, Yangying Ou^{3*}, Ying Yang³, Lu Wang³, Yuwei Zhang³, Fulan Zhao¹, Pixian Shui² and Jie Qing^{3,4} 

¹Department of Pharmacy, The Affiliated Traditional Chinese Medicine Hospital of Southwest Medical University, Luzhou 646000, China; ²Department of Pharmacy, Southwest Medical University, Luzhou 646000, China; ³National Traditional Chinese Medicine Clinical Research Base and Research Center of Integrated Traditional Chinese and Western Medicine, The Affiliated Traditional Chinese Medicine Hospital of Southwest Medical University, Luzhou 646000, China; ⁴MOE Key Laboratory of Bioorganic Phosphorus Chemistry & Chemical Biology, Department of Chemistry, Tsinghua University, Beijing 100084, China

*These authors contributed equally to this paper.

Corresponding authors: Jie Qing. Email: qing282420@163.com; Pixian Shui. Email: 1018989427@qq.com

Impact Statement

The development of *obstructive cholestasis* may cause liver fibrosis and liver failure, for which no effective therapies exist currently. This study found that intrahepatic cholestasis in a mouse model of common bile duct ligation accompanied the activation of the coagulation cascade. An anticoagulatory antagonist of thrombin, hirudin, suppressed pathological angiogenesis and reduced tissue hypoxia and inflammation. *In vivo and in vitro*, hirudin treatment suppresses thrombin-induced profibrotic YAP activity in endothelial cells. Inhibition of coagulation system represents a therapeutic approach for liver obstructive cholestasis and fibrogenesis.

Abstract

Cholestatic fibrogenesis is a pathobiological process in which cumulative injury to the bile ducts coincides with progressive liver fibrosis. The pathobiologic mechanisms underlying fibrogenesis and disease progression remain poorly understood. Currently, there is no effective treatment for liver fibrosis. In this study, we discovered that components of the coagulation cascade were associated with the advanced progression of obstructive cholestasis, and anticoagulant therapy could improve liver cholestasis-induced fibrosis. In a mouse model of common bile duct ligation (BDL), which mimics cholestatic liver injury, RNA sequencing analysis revealed an increased expression of coagulation factors in endothelial cells. Pharmacological targeting of the coagulation signaling by hirudin, an anticoagulatory antagonist of thrombin, ameliorated obstructive cholestasis, and attenuated liver fibrosis symptoms. Hirudin attenuated fibrosis-associated angiogenesis, endothelial-to-mesenchymal transition (EndMT), and tissue hypoxia and reduced liver inflammation after BDL. Furthermore, hirudin suppressed YAP (Yes-associated protein) signaling and its downstream effectors in vascular endothelial cells, which are considered

with profibrotic characteristics. In conclusion, we demonstrated that pharmacological targeting of coagulation signaling by hirudin has the potential to alleviate liver obstructive cholestasis and fibrosis.

Keywords: Cholestatic fibrogenesis, coagulation pathway, hirudin, YAP signaling, endothelial cell, angiogenesis

Experimental Biology and Medicine 2023; 248: 1242–1253. DOI: 10.1177/15353702231191190

Introduction

Chronic or overwhelming liver injury frequently causes dysfunctional repair, which further leads to excessive scar formation and fibrosis.¹ Liver fibrosis is an important cause of cirrhosis and liver failure in chronic liver disease. Cholestatic fibrogenesis is a pathobiological process in which cumulative injury of the bile ducts coincides with progressive biliary fibrosis.² This phenomenon is clinically related to several cholangiopathies, such as primary sclerosing cholangitis and primary biliary cholangitis, both initiated by an inflammation of the biliary system. A well-established murine model

to mimic cholestatic liver injury consists of common bile duct ligation (BDL). Early acute BDL injury is characterized by the initiation of inflammation with immune cell infiltration, while chronic injury, established more than 10 days after surgery, leads to aggravated inflammation and advanced fibrogenesis.³ This pathological process involves not only hepatocytes but also non-parenchymal liver cells, such as endothelial cells, hepatic stellate cells, and immune cells.

During injury, the liver tissues synthesize large amounts of coagulation-related proteins responsible for blood clot formation. The coagulation system involves a complex series of

serine proteases activated by inflammatory signals in response to tissue injury. However, their inappropriate or uncontrolled activation may lead to fibrosis development.⁴ The main coagulation protease is thrombin (factor IIa), which converts plasma fibrinogen into insoluble fibrin clot through proteolysis. Thrombin exerts pro-inflammatory and fibrogenic effects in various pathological contexts, including liver fibrosis,^{5,6} pulmonary fibrosis,^{7,8} and cardiac fibrosis.⁹ It is expressed on the surface of activated platelets and orchestrates cell recruitment in response to tissue injury.¹⁰ It also participates in vascular inflammation through the activation of protease activator receptors (PARs).¹¹ Thrombin plasma level was reported to increase in patients with obesity and non-alcoholic fatty liver disease (NAFLD).¹² One mechanism behind the fibrogenic effect of the coagulation system is the formation of intrahepatic microthrombosis, which may lead to local ischemia, disrupted blood flow, and, ultimately, tissue fibrosis.⁴

Hepatic endothelial cells (ECs) are the second largest cell population in the liver and are predominantly represented by liver sinusoidal endothelial cells (LSECs), which form an instructive vascular niche.^{13–15} ECs provide instructive angiocrine factors that induce the regeneration of adjacent parenchymal cells during liver repair, but their aberrant activation generates profibrotic factors that activate perivascular fibroblasts and cause organ fibrosis.^{16–18} We previously reported that repressing ECs expressing connective tissue growth factor (CTGF) and vascular cell adhesion molecule 1 (VCAM1) or blocking pathological angiogenesis could attenuate liver fibrosis.^{19–21} In this study, we demonstrated that pro-coagulant factors were upregulated in hepatic ECs after BDL and that cholestatic liver development was concomitant with pathological angiogenesis. Hirudin is a natural antagonist of thrombin, universally known for its anticoagulatory properties. It ameliorated obstructive cholestasis and attenuated liver fibrosis symptoms. We further discovered that hirudin treatment blocked pathological angiogenesis and repressed the expression of profibrotic CTGF and VCAM1 in ECs. In addition, pro-coagulant factors such as thrombin activated the profibrotic Yes-associated protein (YAP) and induced angiogenesis, which could be antagonized by hirudin.

Materials and methods

Mouse models

The mouse model of BDL-induced cholestatic liver fibrosis was established as previously described.²² The common bile duct was isolated and ligated during laparotomy under anesthesia. Sham mice underwent an identical surgical incision without ligation. For therapies, 100 μ L hirudin (HARVEYBIO, H34958-100, 20 mg/kg with 10% dimethyl sulphoxide (DMSO) in saline) was administered intraperitoneally to the mice once every 2 days for a total of five injections,²³ and the vehicle was 10% DMSO in saline. Ten days after surgery, the mice were euthanized, and blood and liver samples were collected. All mouse experiments were approved by the Animal Experiment Administration Committee of Southwest Medical University (No. 20211122-093). The experimental procedures and animal welfare requirements were strictly followed.

Immunostaining, histology, protein, and mRNA expression analyses of mouse samples

The experiments were performed as previously described.¹⁹ Serum aspartate aminotransferase (AST) and alanine aminotransferase (ALT) were measured by using dedicated assay kits (C009-2-1 and C010-2-1, Nanjing Jiancheng Bioengineering Institute). For histology, a portion of the liver samples collected was fixed in 10% paraformaldehyde. After embedding the tissues in paraffin, the liver samples were cut into 4- μ m-thick sections. Following subsequent deparaffinization and rehydration, the sections were stained with hematoxylin and eosin (H&E), Masson, and Sirius red solutions.

For immunohistochemistry, after rehydration as described above, the liver sections were boiled in 10 mM sodium citrate buffer (pH 6.0) for 10 min to retrieve antigens. Hydrogen peroxide at 3% concentration was used to inhibit endogenous peroxidase activity. Then, the sections were incubated and blocked in 10% goat serum for 30 min. Primary antibodies were incubated at 4°C overnight. Protein detection was conducted using the two-step universal anti-rabbit/mouse immunohistochemistry kit (ZSGB-BIO, PV-9000). For immunofluorescent staining, after freezing in optimal cutting temperature compound, 6- μ m-thick liver sections were cut and fixed for 10 min in 10% paraformaldehyde. Next, the sections were permeabilized for 10 min in 0.1% Triton X-100 and blocked in 10% goat serum for 30 min. Primary antibodies were incubated overnight at 4°C, and secondary antibodies for 1 h at room temperature. The nuclei were visualized by staining with 4',6'-diamidino-2-phenylindole (DAPI). The information related to the antibodies is shown in Table 1. Data quantification was conducted with ImageJ software.

For mRNA expression analyses, a standard protocol was followed to isolate the total RNA of mouse livers with TRIzol reagent. The gene expression of inflammatory and fibrosis-related factors was measured by quantitative real-time reverse transcription PCR (qRT-PCR) with GAPDH as an internal control. The primer sequences are shown in Table 2. qRT-PCR was conducted with the One Step qRT-PCR SYBR Green Kit (Vazyme, Q221-01), and relative gene expression was calculated according to the $\Delta\Delta$ CT method.

Enzyme-linked immunosorbent assay (ELISA)

Mouse bloods were left at 4°C overnight and serums were collected at 3000 rpm for 15 min. ELISA was performed to detect the protein levels of IL-1 β and IL-6 in serums under the instructions of kits' manufacturer. ELISA kits: Mouse IL-1 beta ELISA Kit (Proteintech, KE10003) and Mouse IL-6 ELISA Kit (Proteintech, KE10007) were used.

Isolation of mouse liver ECs

Fresh liver tissues were collected, finely minced, and digested in 2 mg/mL collagenase A at 37°C. The cells were dissociated mechanically with an 18G syringe, filtered, and centrifuged to obtain a single cell suspension. Next, erythrocytes were removed by treating the cell pellet with a red blood cell lysing reagent. After washing, centrifugation, and resuspension in Dulbecco's phosphate buffered saline (DPBS), the single cell

Table 1. Antibody Information.

Name	Citation	Supplier	Cat no.	Clone no.
Anti-F4/80	PMID: 32157317	Abcam	ab6640	Cl: A3-1
Smooth Muscle Actin	PMID: 35719213	Proteintech	80008-1-RR	5H7
Anti-YAP1	PMID: 32728211	Proteintech	13584-1-AP	Polyclonal
Anti-WWTR1(TAZ)	PMID: 29438698	Proteintech	23306-1-AP	Polyclonal
Anti-CTGF	PMID: 35563783	Santa	sc-365970	E-5
Anti-VCAM-1	PMID: 34894925	Santa	sc-13160	E-10
Anti-HIF-1 alpha	PMID: 32599679	Abcam	ab179483	EPR16897
CA9 antibody	PMID: 31705175	Proteintech	11071-1-AP	Polyclonal
FSP1(S100A4)	PMID: 29248714	Proteintech	16105-1-AP	Polyclonal
Anti-IL-1 Beta	PMID: 30405119	Proteintech	16806-1-AP	Polyclonal
Anti-Mouse CD31	PMID: 7956830	BD Biosciences	553370	MEC 13.3
Anti-Mouse IL-6	PMID: 33414464	Proteintech	66146-1-Ig	1A3B4
Anti-LYVE1	PMID: 34648896	Fitzgerald	70R-LR003	Polyclonal
COL1A1	PMID: 36594034	Cell Signaling Technology	72026T	E8F4L
Goat Anti-Mouse IgG (Alexa Fluor® 488)	PMID: 35778954	Abcam	ab150113	Polyclonal
Goat Anti-Rabbit IgG (Alexa Fluor® 488)	PMID: 33474514	Abcam	ab150081	Polyclonal
Goat Anti-Mouse IgG (Alexa Fluor® 555)	PMID: 33530637	Abcam	ab150114	Polyclonal
Goat Anti-Rat IgG (Alexa Fluor® 555)	PMID: 31659300	Abcam	ab150158	Polyclonal

Table 2. All Primers Used for qRT-PCR.

Name of primers	Sequences
GAPDH-F (forward)	5'-CCCCTCCCTCCACCTTTGACG-3'
GAPDH-R (reverse)	5'-CACCACCCTGTTGCTGTAGCCA-3'
Cyclin D1F	5'-CCCTCGGTGCCTACTTCA-3'
Cyclin D1-R	5'-CCTCGCACTTCTGTTCCCTC-3'
Cyclin D2F	5'-GAACAGAAGTGCGAAGAAG-3'
Cyclin D2-R	5'-GGAGTTGTCGGTGTAATG-3'
Cyclin D3F	5'-GGAGGTATGTGAGGAGCAGC-3'
Cyclin D3-R	5'-AGCGTGGTCCGGTGTAGATG-3'
mouse-GAPDH-F (forward)	5'-GTGCCGCCTGGAGAAACCT-3'
mouse-GAPDH-R (reverse)	5'-TGAAGTCGCAGGAGACAACC-3'
mouse-IL1β-F	5'-TGCCACCTTTGACAGTGATG-3'
mouse-IL1β-R	5'-AAGGTCCACGGGAAAGACAC-3'
mouse-IL6F	5'-TAACCACCCCTGACCCAACC-3'
mouse-IL6-R	5'-CATTTGCCGAAGAGCCCTCA-3'
mouse-αSMA-F	5'-AAGTATCCGATAGAACACG-3'
mouse-αSMA-R	5'-TCAAACATAATCTGGGTCA-3'
mouse-Collagen I-F	5'-ACGCCATCAAGGTCTACTGC-3'
mouse-Collagen I-R	5'-ACGGGAATCCATCGGTTCAT-3'

suspension was incubated in a shaker using Dynabeads™ sheep anti-Rat IgG magnetic beads (Invitrogen, 11035) conjugated with rat anti-mouse CD31 antibody for 4h at 4°C. The bead-bound liver ECs were sorted by using a magnetic rack and collected with DPBS.

Treatment of human umbilical vein endothelial cells (HUVECs) with hirudin

HUVECs were provided by Prof. Bi-sen Ding's Lab of Sichuan University and cultured in the primary endothelial cell culture medium (PriMed-icell-002, iCellbioscience). HUVECs were seeded in 12-well plates and cultured overnight at 37°C. The following day, the cells were stimulated with thrombin (10 U, 5 U, or 1 U, HARVEYBIO, PN1083) and exposed to hirudin at different concentrations (2 U, 1 U) for 24 h. Part of the culture was stained with anti-YAP antibody

to assess cellular localization. Other cells were collected for mRNA extraction using TRIzol. The mRNA level of cyclin D1, D2, and D3 was determined by qRT-PCR as described above, with GAPDH expression used as an internal control. The primer sequences are shown in Table 2.

Tube formation assay

The tube formation assay was conducted on HUVECs to examine endothelial tube formation.²⁴ Matrigel (Corning, 356234) was completely thawed at 4°C and mixed with a complete medium of the primary endothelial cell culture system (1:1). 200 μL matrigel mixture was coated into the 24-well plates, and the plate was incubated at 37°C for 1h to allow matrigel solidification. Then 300 μL HUVECs in complete medium or additionally treated with thrombin, hirudin or verteporfin were added on top of the matrix (2 × 10⁵ cells/well). After incubated for 6-12 h at 37°C, tube formation was observed and captured with an inverted microscope.

Statistical analysis

Statistical analysis was conducted using the software GraphPad Prism 6. The data are expressed as mean values ± standard deviations (SD). The two-group comparisons were assessed by a two-tailed *t*-test, while multiple-group comparisons were evaluated by one-way ANOVA, followed by Tukey's or Dunnett's test. Animal survival rate was evaluated by the Kaplan-Meier estimator, and comparing differences between groups was based on log-rank statistics. The significant threshold was *P* value < 0.05, while the highly significant level was *P* value < 0.01 (**P* < 0.05; ***P* < 0.01).

Results

Obstructive cholestasis activated the coagulation system in mouse liver

To study the molecular changes accompanying liver fibrosis, we used a mouse model of BDL, which mimics obstructive

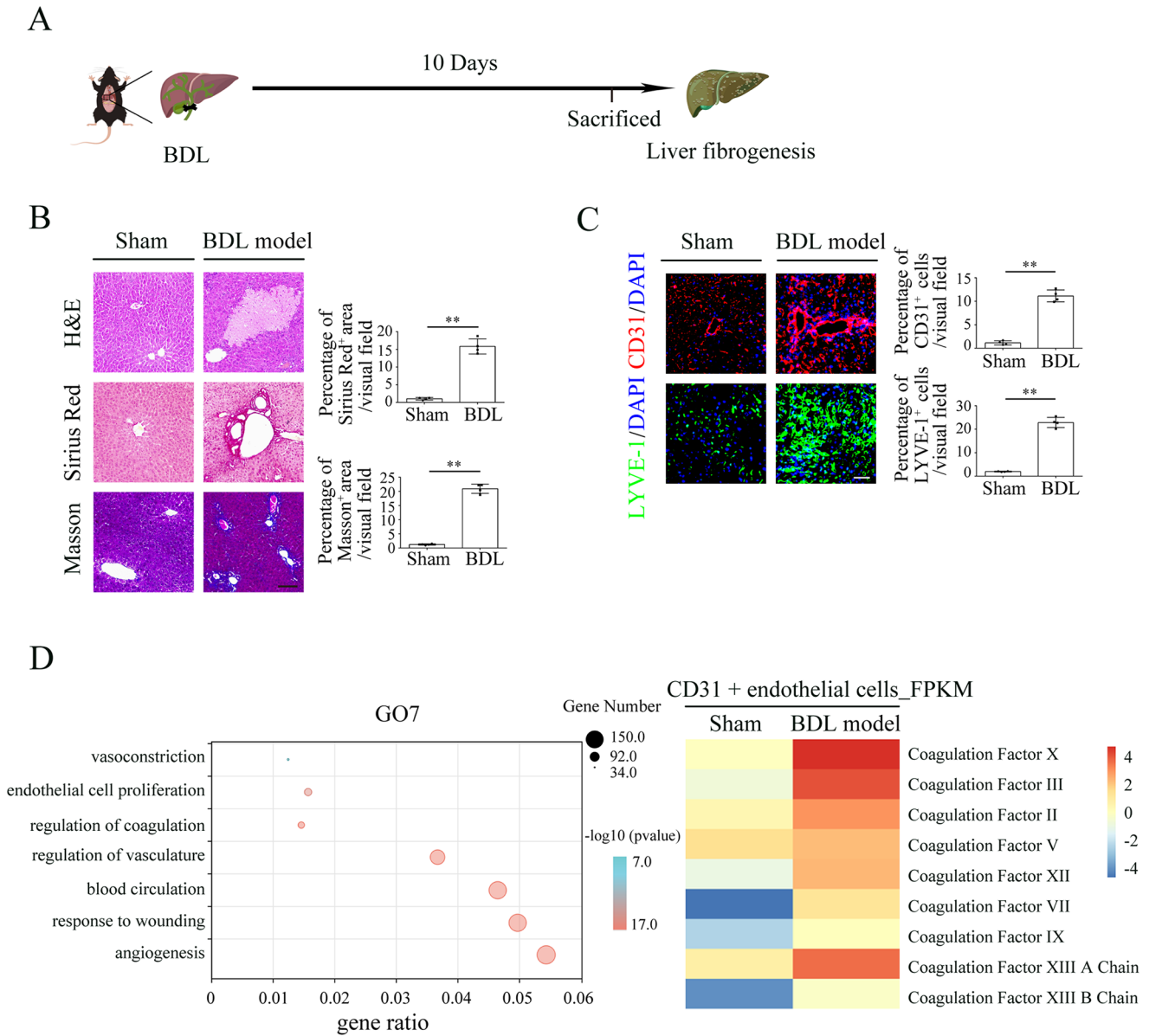


Figure 1. Common bile duct ligation (BDL)-induced obstructive cholestasis activates the expression of coagulation factors in endothelial cells (ECs). (A) Schematic representation of the establishment of BDL-induced liver obstructive cholestasis in mice. (B) H&E, Masson, and Sirius red staining of mouse liver sections from sham or BDL mice; bar charts summarize the staining quantification ($n=4$ mice/group). (C) Immunofluorescent staining of mouse liver sections from the sham or BDL mice and quantification of LYVE-1 (green, sinusoidal endothelial cell marker) or CD31 (red, vascular endothelial cell marker) positive cells. (D) Gene Ontology (GO) enrichment analysis and heat map of coagulation factors obtained by RNA sequencing analysis of CD31⁺ ECs isolated from sham or BDL-induced mouse livers. Scale bars, 100 μ m (B) and 50 μ m (C). All results are presented as the mean \pm SD. FPKM: Fragments per kilobase of transcript per million fragments mapped. * $P < 0.05$, ** $P < 0.01$. (A color version of this figure is available in the online journal.)

cholestasis (Figure 1(A)). After ligation of the common bile duct, the liver enlarged symmetrically and exhibited obstructive cholestasis. Histological analysis using H&E showed an increased amount of bile infarcts in ligated mice. Staining of the liver sections with Masson and Sirius red revealed the occurrence of liver fibrosis and thrombosis (Figure 1(B)). Immunofluorescence analysis of the endothelial marker CD31 and sinusoidal endothelial marker LYVE-1 showed increased angiogenesis during BDL-induced obstructive cholestasis (Figure 1(C)). Furthermore, gene expression analysis by RNA sequencing (RNA-seq) in the liver ECs isolated from BDL-induced or sham mice showed a significant upregulation of

the coagulation factors during obstructive cholestasis (Figure 1(D)). Further investigation on whether the activation of the coagulation system by obstructive cholestasis contributed to liver injury and pathological angiogenesis is needed.

The anticoagulant hirudin ameliorated obstructive cholestasis and attenuated liver fibrosis symptoms

Hirudin exerts its anticoagulant effect by blocking thrombin's anion binding site. This effect operates not only on soluble thrombin but also on thrombus-bound thrombin.²⁵ These properties prompted us to test whether hirudin could

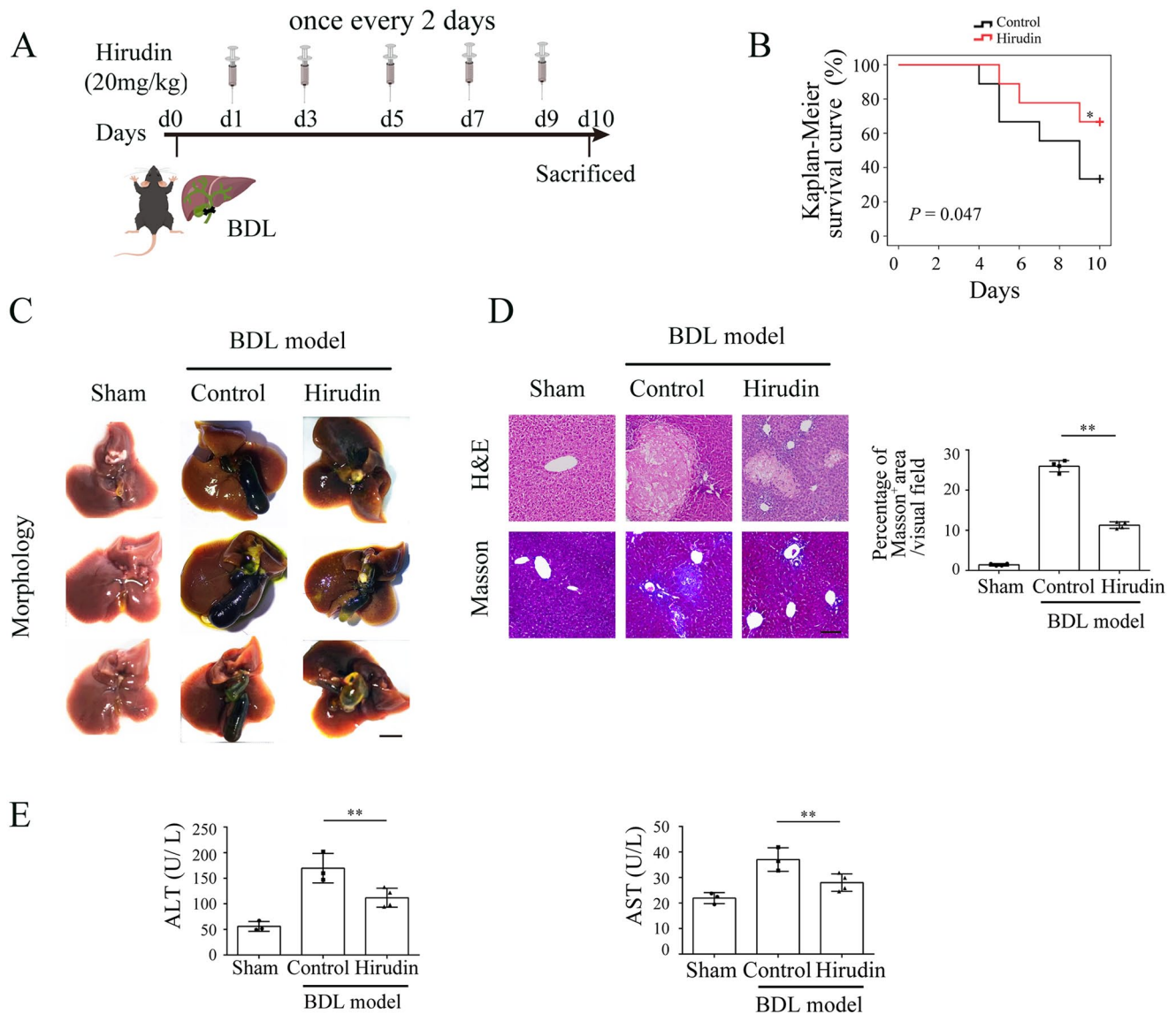


Figure 2. Hirudin ameliorates cholestatic liver injury. (A) Schema summarizing the experimental setup to assess hirudin efficacy in BDL-induced obstructive cholestasis. (B) Survival rate of mice under BDL-induced obstructive cholestasis in the control and hirudin-treated groups is shown by Kaplan–Meier analysis ($n=9$ mice per group). One representative survival analysis in two independent experiments. (C) Liver and gallbladder morphological alterations induced by BDL in the indicated groups. (D) H&E and Masson staining of liver sections from sham-operated, BDL-induced, and hirudin-treated BDL-induced mice ($n=4$ mice/group). (E) Determination of serum AST and ALT activity ($n=3-4$ mice/group). Scale bars, 500 μm (C) and 100 μm (D). All results are presented as the mean \pm SD. * $P < 0.05$, ** $P < 0.01$.

serve as a therapeutic agent for BDL-induced liver injury (Figure 2(A)). Mice with BDL-induced obstructive cholestasis and treated with hirudin exhibited a higher survival rate than untreated counterparts (Figure 2(B)). Ten days postsurgery, gall bladder enlargement, accompanied with jaundice and liver swelling, was observed in BDL mice, but these symptoms were considerably improved in the hirudin-treated group (Figure 2(C)). Further analysis by H&E and Masson staining showed that hirudin reduced the necrotic area and thrombosis. Meanwhile, the livers from the treated mice showed decreased obstructive cholestasis (Figure 2(D)). Serum AST and ALT levels indicated attenuated liver injury in hirudin-treated mice (Figure 2(E)). The amounts of smooth muscle alpha-actin (α -SMA), collagen I deposition, and Sirius red staining in the liver were also reduced by

the treatment, indicating that hirudin could reduce hepatic fibrosis (Figure 3(A) to (C)). The mitigation of liver fibrosis by hirudin suggested that targeting the coagulation system has the potential to improve liver obstructive cholestasis and fibrogenesis.

Hirudin reduced liver inflammation after BDL-induced liver obstructive cholestasis

It was previously reported that EC-specific anticoagulation reduced inflammation in acute lung injury.⁷ Here, F4/80-positive areas (pan-macrophage marker) in the liver sections from BDL-induced mice were increased compared with those of mice from the sham group. However, F4/80-positive areas were reduced in the livers of hirudin-treated

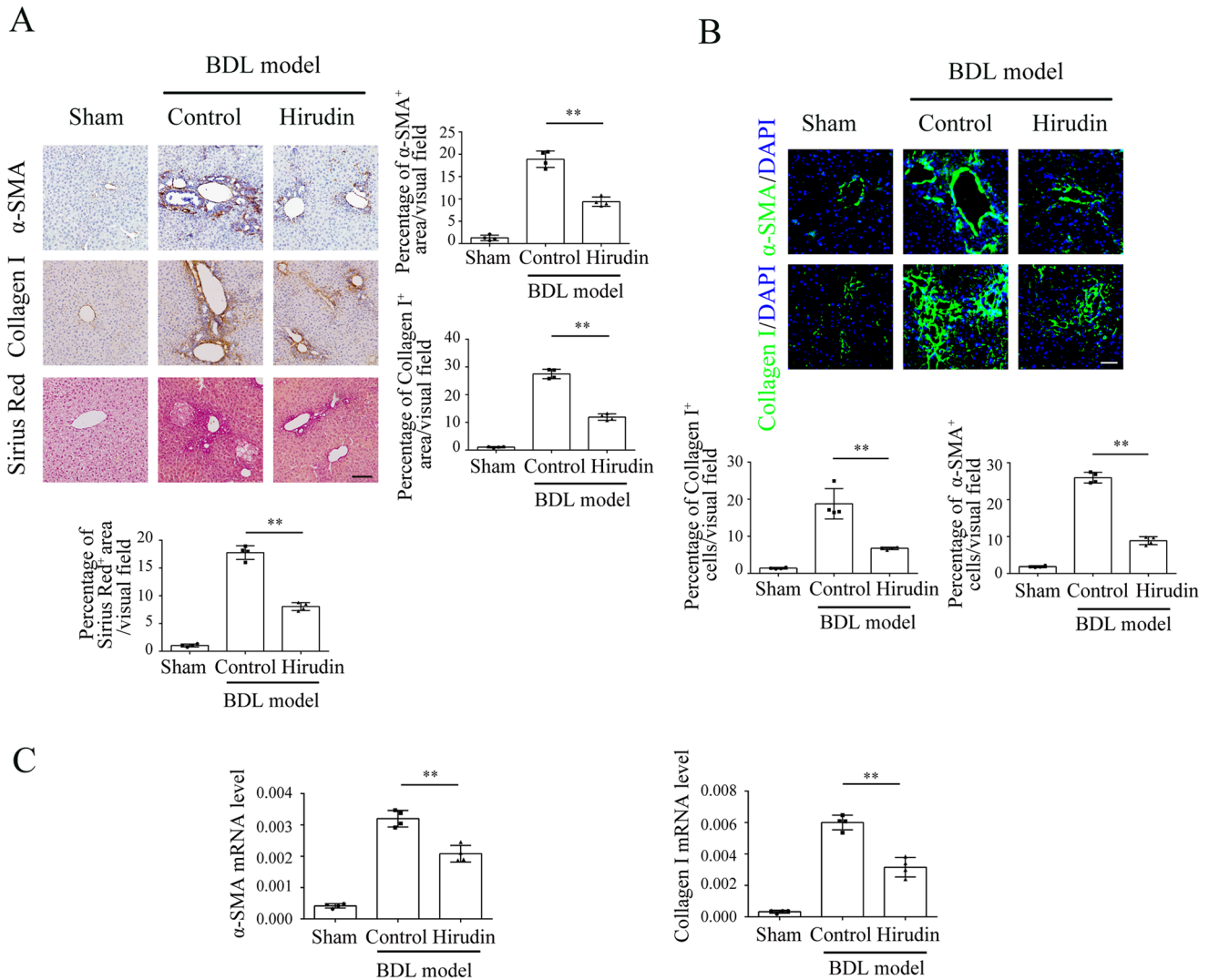


Figure 3. Hirudin reduces BDL-induced liver fibrosis. (A) Immunohistochemistry against α -SMA and collagen I, and Sirius red staining and quantification from the liver sections of sham-operated, BDL-induced, and hirudin-treated BDL-induced mice ($n=4$ mice/group). (B) Immunofluorescent staining against α -SMA and collagen I was performed on mouse liver sections ($n=4$ mice/group). (C) mRNA expression of α -SMA and collagen I ($/GAPDH$) in the liver tissues from the indicated groups ($n=4$ mice/group), as determined by RT-qPCR. Scale bars, 100 μ m (A) and 50 μ m (B). All results are presented as the mean \pm SD. * $P < 0.05$, ** $P < 0.01$.

mice (Figure 4(A)). Furthermore, we found that the levels of several pro-inflammatory cytokines assessed by immunofluorescence, including IL-1 β and IL-6, were lower in the livers of the hirudin-treated mice than in those from the untreated group (Figure 4(A)). The ability of hirudin to dampen BDL-induced IL-1 β and IL-6 in the liver was confirmed at the mRNA level by qRT-PCR and at the protein level by measuring serum IL-1 β and IL-6 by ELISA (Figure 4(B) and (C)). Altogether, these data showed that hirudin treatment reduces liver inflammation after BDL-induced liver obstructive cholestasis.

Hirudin attenuated fibrosis-associated angiogenesis, endothelial-to-mesenchymal transition (EndMT), and tissue hypoxia

Immunofluorescence analysis of CD31 expression showed that hirudin prevented angiogenesis in BDL-induced

obstructive cholestasis. CTGF and VCAM1 are considered profibrogenic, and their expression in liver ECs was upregulated upon BDL in mouse, which was reversed by treatment with hirudin (Figure 5(A)). EndMT is a cellular transdifferentiation program during which ECs acquire some mesenchymal features.²⁶ EndMT was assessed by co-staining endothelial (CD31) and mesenchymal markers (α -SMA, FSP1). This analysis showed that the proportion of ECs undergoing EndMT was significantly reduced in hirudin-treated mice compared to controls (Figure 5(B)). Thus, hirudin could limit pathological angiogenesis.

Inadequate blood perfusion caused by coagulation and EndMT may result in inadequate oxygen tension, which leads to parenchymal hypoxia in injured tissues.^{26,27} Thus, we tested whether treatment with anticoagulant could limit tissue hypoxia during BDL-induced liver fibrosis. Immunofluorescence analysis revealed that ECs in BDL-induced livers showed high expression of carbonic

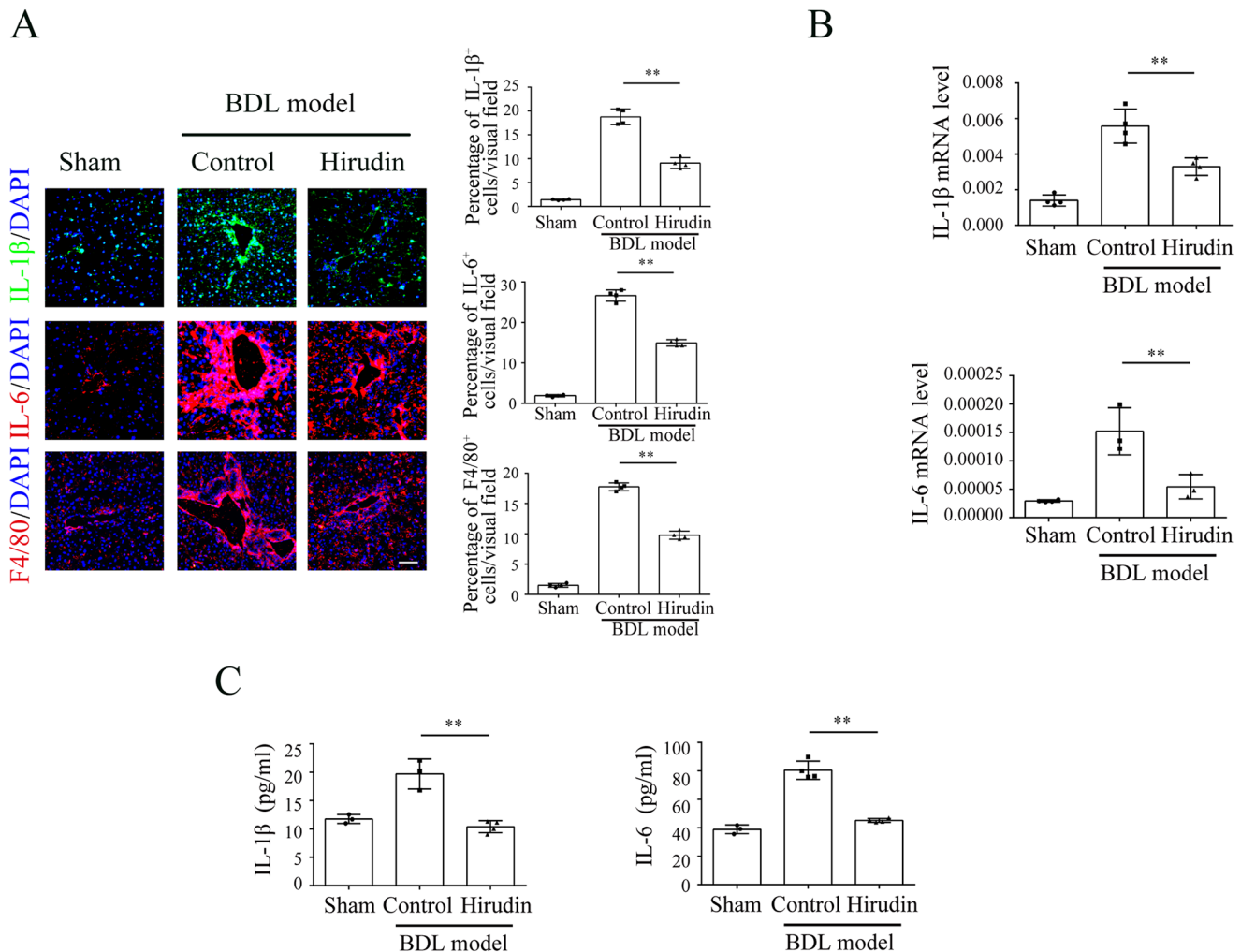


Figure 4. Hirudin treatment attenuates the liver inflammation induced by obstructive cholestasis. (A) Immunofluorescent staining of mouse liver sections from the indicated groups against inflammatory markers (IL-1 and IL-6) or pan-macrophage marker (F4/80) ($n=4$ mice/group). (B) IL-1 β and IL-6 mRNA levels (/GAPDH) in the liver tissues. (C) Quantitative analysis of serum IL-1 β and IL-6 by ELISA ($n=3-4$ mice/group). Scale bars, 50 μ m (A). All results are presented as the mean \pm SD. * $P < 0.05$, ** $P < 0.01$.

anhydrase IX (CAIX), a marker of hypoxia,²⁶ and that CAIX was inhibited in hirudin-treated mice (Figure 5(C)). The hypoxic response was further demonstrated by assessing the nuclear stabilization of the hypoxia transcription factor HIF1 α . Similarly, hirudin decreased the expression of HIF1 α in BDL mice (Figure 5(C)). These results suggested that hirudin could ameliorate tissue hypoxia in the BDL model.

Hirudin suppressed YAP signaling in vascular ECs activated by coagulation

We previously reported that the genetic deletion of YAP in ECs inhibited the emergence of EndMT and ameliorated organ fibrosis.²⁰ To identify the cellular targets of hirudin during pathological angiogenesis and EndMT, we measured YAP and its paralog TAZ *in vivo*. In mouse BDL-induced liver obstructive cholestasis, immunofluorescence analysis showed an increased expression of endothelial YAP (CD31⁺ YAP⁺) compared with sham mice, which was suppressed by hirudin treatment, and TAZ protein exhibited

the same change trend as YAP *in vivo* (Figure 6(A)). The upregulation of YAP target genes such as CTGF after BDL in liver ECs was reversed by treatment with hirudin (Figure 5(A)), which indicates that YAP signaling is suppressed by hirudin *in vivo*. To further test the cellular effect of hirudin, primary HUVECs were stimulated with thrombin and exposed to hirudin (Figure 6(B)). In experiment of *in vitro* angiogenesis, we observed that the pro-angiogenic ability and tube formation of thrombin was significantly attenuated by hirudin or a YAP inhibitor verteporfin (Figure 6(C)). Immunofluorescence imaging showed that thrombin-induced the expression and nuclear translocation of YAP in HUVECs, which was reduced by hirudin treatment (Figure 6(D)). Furthermore, hirudin reduced the expression of cyclin D1, D2, and D3, which represent key cell cycle regulators acting downstream of YAP signaling (Figure 6(E)). We cannot rule out the possibility that hirudin treatment may affect other cellular functions. These results support that hirudin treatment suppresses thrombin-induced profibrotic YAP activity and proliferation in ECs.

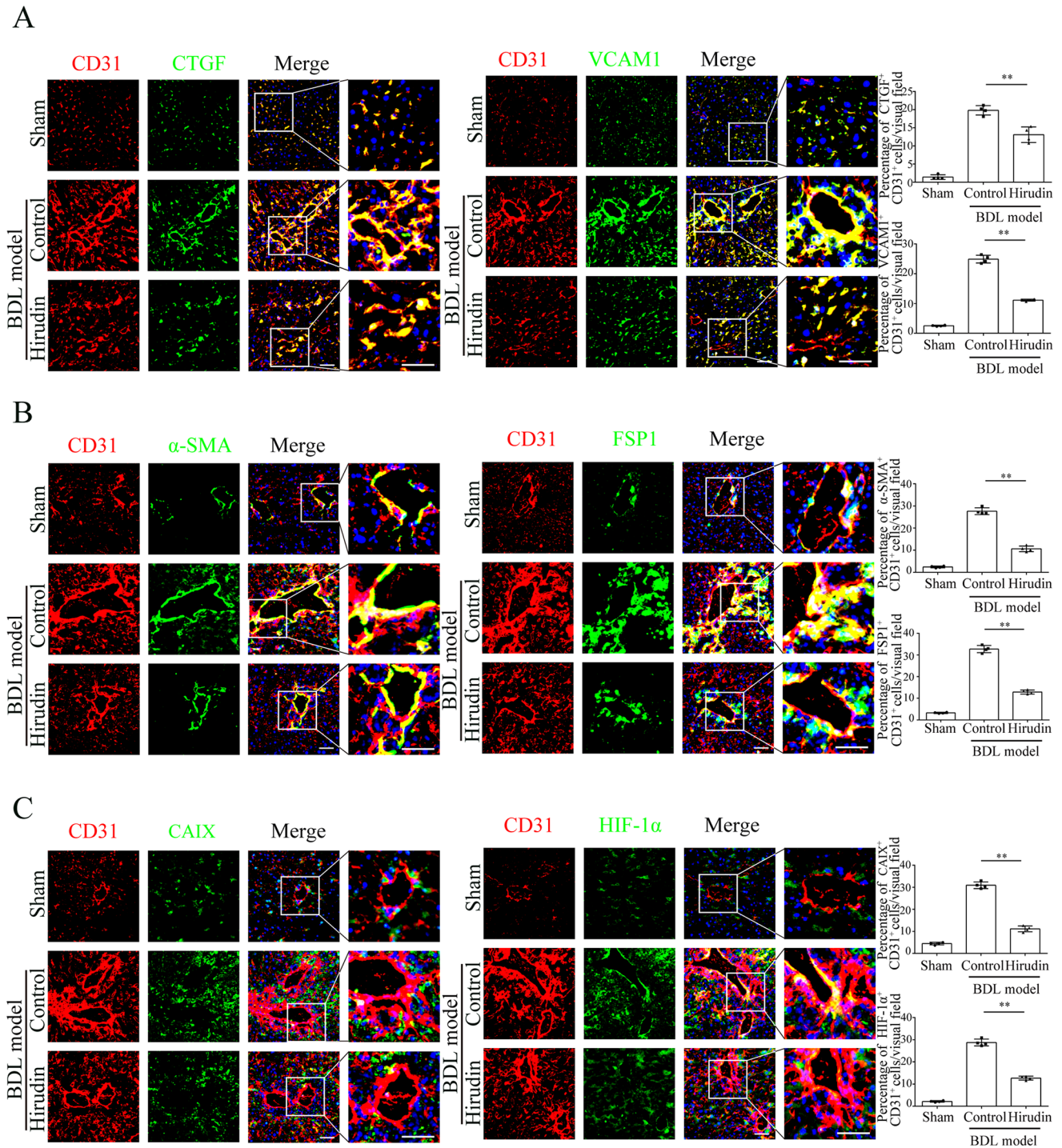


Figure 5. Hirudin alleviates liver fibrosis-associated angiogenesis, endothelial-to-mesenchymal transition (EndMT), and tissue hypoxia. (A) Immunofluorescent co-staining of liver tissue sections for CD31 (red) and the profibrogenic proteins CTGF or VCAM1 (green). The bar charts show the quantitative analysis of the positive cell areas for each marker ($n=4$ mice/group). (B) Immunofluorescent co-staining of liver tissue sections for CD31 (red) and the mesenchymal markers α -SMA or FSP1 (green), and corresponding quantification ($n=4$ mice/group). (C) Immunofluorescent co-staining of liver tissue sections for CD31 (red) and the hypoxia markers CAIX and HIF-1 α (green), and corresponding quantification ($n=4$ mice/group). Scale bars, 50 μ m (A) to (C). All results are presented as the mean \pm SD. * $P < 0.05$, ** $P < 0.01$. (A color version of this figure is available in the online journal.)

Discussion

Prothrombotic states exert pro-inflammatory and profibrotic effects that promote fibrosis and induce angiogenesis in the liver, kidney, and lungs.⁹ They result in fibrin accumulation and increased vascular permeability, which lead to leakage of

plasma containing the coagulation factor zymogen into tissues compartment.²⁸ The coagulation factor proteases trigger cell activation and exert pro-inflammatory functions through the cleavage of G protein-coupled PARs, including PAR-1, PAR-2, PAR-3, and PAR-4.²⁹ PARs are implicated in a large number of processes and diseases, including hemostasis,

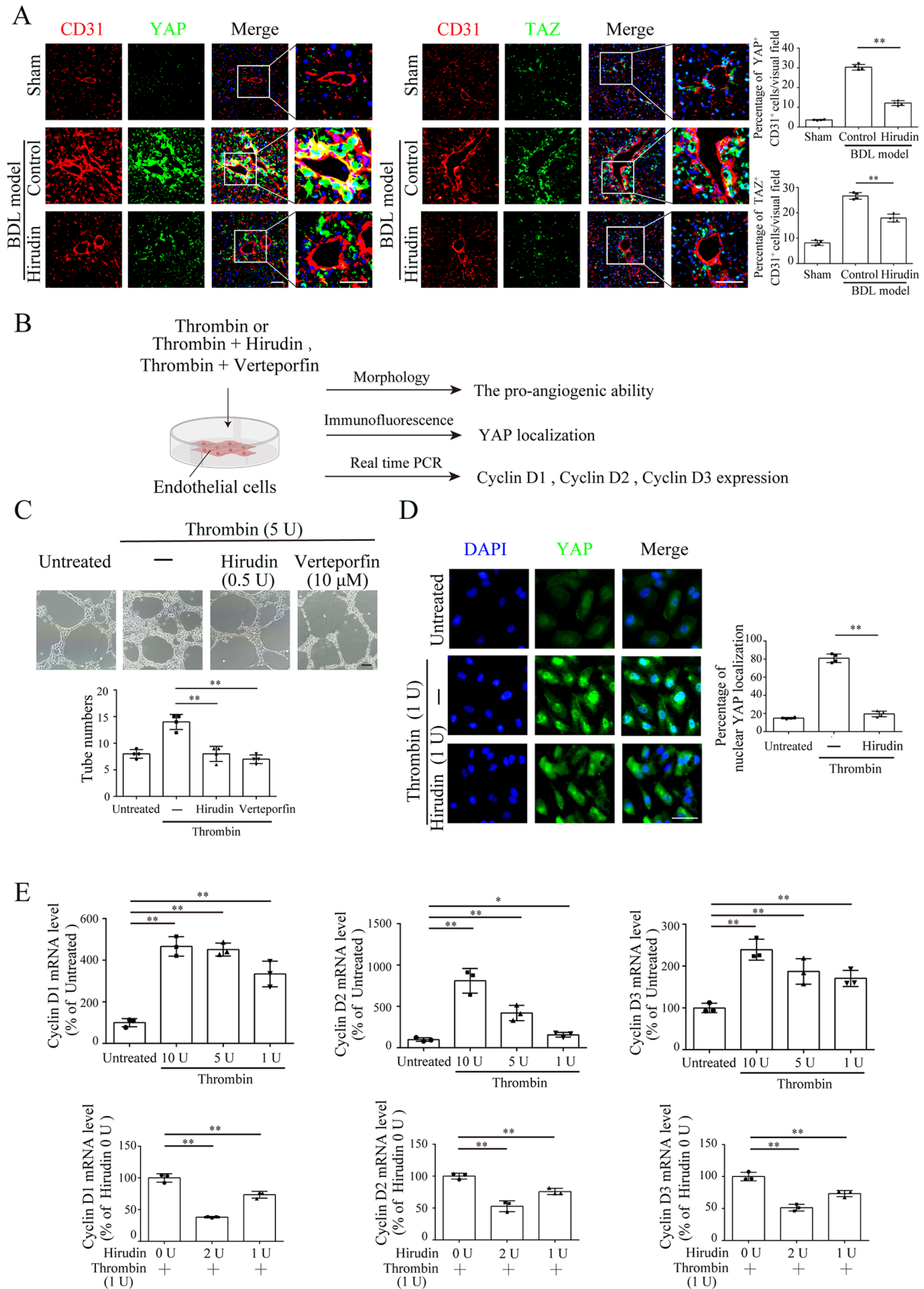


Figure 6. Hirudin suppresses thrombin-induced endothelial YAP activation. (A) Immunofluorescent co-staining of liver tissue sections for CD31 (red) and the profibrogenic protein YAP or TAZ (green) and corresponding quantification ($n=4$ mice/group). (B) Experimental setup to assess the efficacy of hirudin in thrombin-induced endothelial activation. (C) Determination of the effect of hirudin or verteporfin on thrombin-induced endothelial proliferation and tubulogenesis in HUVECs. (D) Analyzing the effect of hirudin on thrombin-induced YAP nuclear localization in HUVECs, and corresponding quantification. (E) Effect of thrombin or additional treatment with hirudin on the mRNA expression of YAP downstream signaling cyclin D1, D2, and D3 in HUVECs. mRNA levels were measured by qRT-PCR. Scale bars, 50 μm (A) and 10 μm (C), (D). All results are presented as the mean \pm SD. * $P < 0.05$, ** $P < 0.01$.

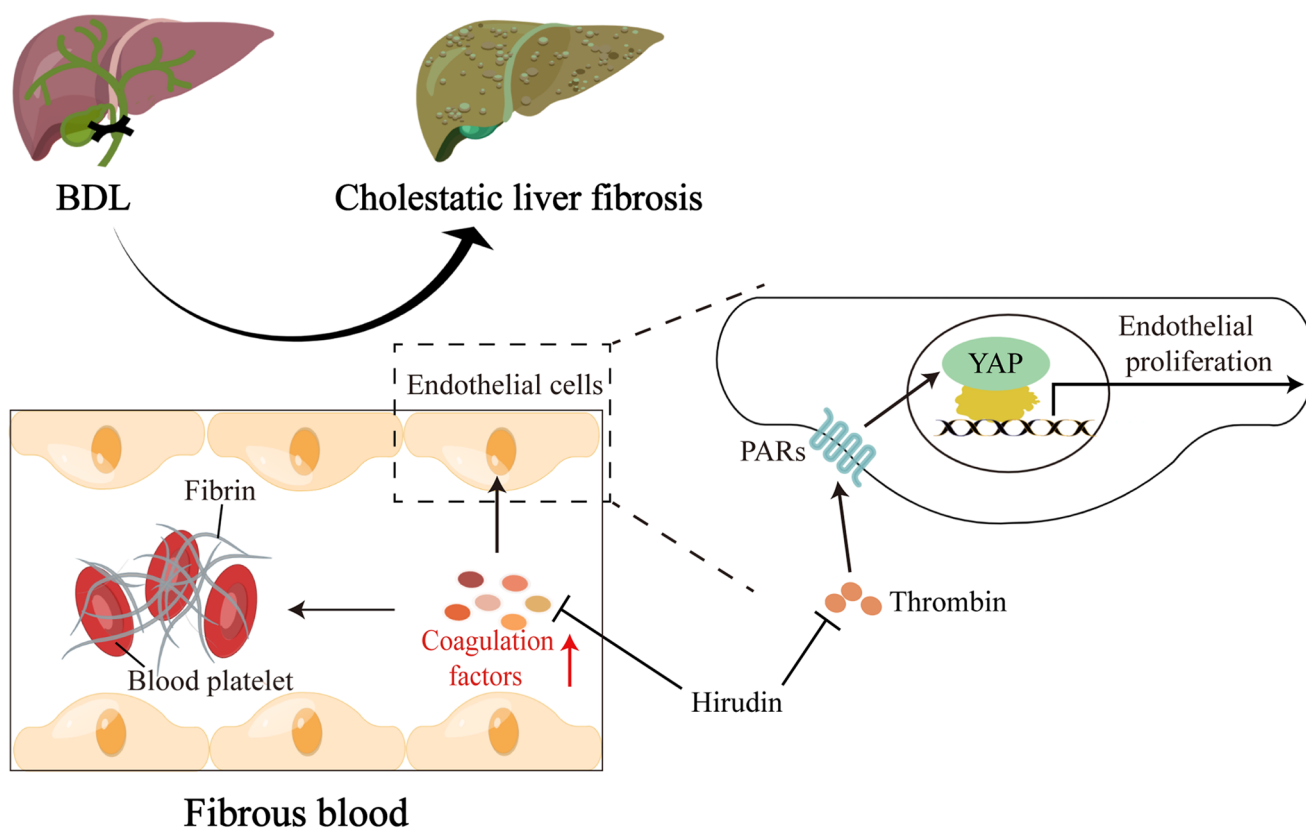


Figure 7. Schematic illustration that hirudin ameliorates liver obstructive cholestasis and fibrosis. After obstructive cholestasis, the liver tissues synthesize large amounts of coagulation-related proteins responsible for blood clot formation. Pharmacological inhibition of the coagulation signaling by hirudin reduces obstructive cholestasis and diminishes liver fibrosis symptoms in a mouse model. In vascular endothelial cells, hirudin could reverse the upregulation of thrombin-induced YAP and restrain dysfunctional angiogenesis.

thrombosis, and inflammation.⁴ PAR-1 is the primary receptor for thrombin. Liver fibrosis is reduced in PAR-1-deficient mice, and administration of PAR-1 antagonist improves liver fibrosis.^{30,31} Several studies indicate that PAR-2 also contributes to liver fibrosis,^{32,33} and we previously reported that a PAR-2 peptide antagonist ameliorated liver and kidney fibrosis.^{20,21} However, the opposite effect was also reported, that is, PAR-4 deficiency could increase serum bile acid concentration and exacerbate hepatocellular injury and peribiliary fibrosis.³⁴ Therefore, collectively, there is strong experimental evidence that inhibiting coagulation proteases through PAR activation is a potential anti-fibrosis strategy.

The Hippo signal pathway is highly conserved in mammals and mainly comprises the serine-threonine protein kinases MST1/2, large tumor suppressor kinases LATS1/2, and the transcriptional co-activators YAP/TAZ.³⁵ The Hippo pathway has emerged as a major player in many aspects of hepatic function, such as liver development, regeneration from injury, and cancer. Aberrant activation of YAP has been associated with chronic liver disease, including the development of liver fibrosis and tumorigenesis.³⁶ YAP plays multifaceted roles in endothelial behaviors and regulates the proliferation of ECs, as well as their metabolic activity during sprouting angiogenesis, vascular barrier formation, and maturation.³⁷ Genetic deletion of vascular endothelial YAP reduces pathological angiogenesis and relieves vascular inflammation.²⁰ Endothelial YAP activity could be regulated

by several pathways, including G protein-coupled receptors (GPCRs). Stimulation of PARs activates YAP by decreasing phosphorylation and increasing its nuclear localization. Activation of PAR1 and other GPCRs can lead to aberrant cell growth through $G_{12/13}$ -coupled receptors that inhibit the Lats1/2 kinases and activate YAP.^{38,39} We previously reported that the peptide antagonist FSLRLY-NH2 selectively blocked PAR2/YAP activity in ECs and ameliorated liver and kidney fibrosis.^{20,21}

Cholestatic liver injury leads to liver inflammation and fibrosis, and the mechanisms associated with disease progression are still not fully understood.³ In this study, we discovered that pro-coagulant factors were upregulated in hepatic ECs after BDL. Anticoagulatory antagonist hirudin ameliorated obstructive cholestasis and liver fibrosis. In addition, hirudin blocked the profibrotic activity of endothelial YAP and suppresses pathological angiogenesis (Figure 7). Targeting coagulation signaling has the potential to help develop new therapeutic approaches for cholestatic liver injury.

AUTHORS' CONTRIBUTIONS

All authors participated in the design, interpretation of the studies and analysis of the data. JQ and XY designed the study and wrote the manuscript. XY, YYO, YY, LW, and YWZ performed experiments. PXS and FLZ revised the manuscript. JQ and PXS supervised and supported the research financially.

DECLARATION OF CONFLICTING INTERESTS

The author(s) declared no potential conflicts of interest with respect to the research, authorship, and/or publication of this article.

FUNDING

The author(s) disclosed receipt of the following financial support for the research, authorship, and/or publication of this article: This work was supported by the National Natural Science Foundation of China (grant nos. 22077106 and 81700542); Sichuan Science and Technology Program (grant no. 2020JDRC0113); Natural Science Project of Southwest Medical University (grant nos. 2021ZKMS054 and 2021ZKQN131); and Innovation Team and Talents Cultivation Program of National Administration of Traditional Chinese Medicine (grant no. ZZYCXTD-C-202207).

ORCID ID

Jie Qing  <https://orcid.org/0000-0002-2618-1984>

REFERENCES

- Gurtner GC, Werner S, Barrandon Y, Longaker MT. Wound repair and regeneration. *Nature* 2008;**453**:314–21
- Jalan-Sakrikar N, De Assuncao TM, Shi G, Aseem SO, Chi C, Shah VH, Huebert RC. Proteasomal degradation of enhancer of zeste homologue 2 in cholangiocytes promotes biliary fibrosis. *Hepatology* 2019;**70**:1674–89
- Frissen M, Liao L, Schneider KM, Djurdjaj S, Haybaeck J, Wree A, Rolke-Kampczyk U, von Bergen M, Latz E, Boor P, Trautwein C. Bidirectional role of NLRP3 during acute and chronic cholestatic liver injury. *Hepatology* 2021;**73**:1836–54
- Pant A, Kopec AK, Luyendyk JP. Role of the blood coagulation cascade in hepatic fibrosis. *Am J Physiol-Gastr L* 2018;**315**:G171–6
- Dhar A, Sadiq F, Anstee QM, Levene AP, Goldin RD, Thursz MR. Thrombin and factor Xa link the coagulation system with liver fibrosis. *BMC Gastroenterol* 2018;**18**:60
- Duplantier JG, Dubuisson L, Senant N, Freyburger G, Laurendeau I, Herbert JM, Desmoulière A, Rosenbaum J. A role for thrombin in liver fibrosis. *Gut* 2004;**53**:1682–7
- Lou J, Hu Y, Wu MD, Che LQ, Wu YF, Zhao Y, Tian BP, Bao ZQ, Zhu C, Wu YP, He LL, Bai CX, Zhou J, Ying SM, Li W, Chen ZH, Chen DX, Dorling A, Shen HH. Endothelial cell-specific anticoagulation reduces inflammation in a mouse model of acute lung injury. *Acta Pharmacol Sin* 2019;**40**:769–80
- Hernandez-Rodriguez NA, Cambrey AD, Harrison NK, Chambers RC, Gray AJ, Southcott AM, duBois RM, Black CM, Scully MF, McNulty RJ, Laurent GJ. Role of thrombin in pulmonary fibrosis. *Lancet* 1995;**346**:1071–3
- Dong A, Mueller P, Yang F, Yang L, Morris A, Smyth SS. Direct thrombin inhibition with dabigatran attenuates pressure overload-induced cardiac fibrosis and dysfunction in mice. *Thromb Res* 2017;**159**:58–64
- Bitto N, Liguori E, La Mura V. Coagulation, microenvironment and liver fibrosis. *Cells* 2018;**7**:85
- Popovic M, Smiljanic K, Dobutovic B, Syrovets T, Simmet T, Ise-novic ER. Thrombin and vascular inflammation. *Mol Cell Biochem* 2012;**359**:301–13
- Potze W, Siddiqui MS, Boyett SL, Adelmeijer J, Daita K, Sanyal AJ, Lisman T. Preserved hemostatic status in patients with non-alcoholic fatty liver disease. *J Hepatol* 2016;**65**:980–7
- Ramachandran P, Dobie R, Wilson-Kanamori JR, Dora EF, Henderson BEP, Luu NT, Portman JR, Matchett KP, Brice M, Marwick JA, Taylor RS, Efremova M, Vento-Tormo R, Carragher NO, Kendall TJ, Fallowfield JA, Harrison EM, Mole DJ, Wigmore SJ, Newsome PN, Weston CJ, Iredale JP, Tacke F, Pollard JW, Ponting CP, Marioni JC, Teichmann SA, Henderson NC. Resolving the fibrotic niche of human liver cirrhosis at single-cell level. *Nature* 2019;**575**:512–8
- Xiong XL, Kuang H, Ansari S, Liu TY, Gong JK, Wang S, Zhao XY, Ji YW, Li C, Guo L, Zhou LK, Chen ZM, Leon-Mimila P, Chung MT, Kurabayashi K, Opp J, Campos-Perez F, Villamil-Ramirez H, Canizales-Quinteros S, Lyons R, Lumeng CN, Zhou BY, Qi L, Huertas-Vazquez A, Lusic AJ, Xu XZS, Li SM, Yu YH, Li JZ, Lin JD. Landscape of intercellular crosstalk in healthy and NASH liver revealed by single-cell secretome gene analysis. *Mol Cell* 2019;**75**:644–60
- Sun X, Harris EN. New aspects of hepatic endothelial cells in physiology and nonalcoholic fatty liver disease. *Am J Physiol Cell Physiol* 2020;**318**:C1200–13
- Rafii S, Butler JM, Ding BS. Angiocrine functions of organ-specific endothelial cells. *Nature* 2016;**529**:316–25
- Ding BS, Nolan DJ, Butler JM, James D, Babazadeh AO, Rosenwaks Z, Mittal V, Kobayashi H, Shido K, Lyden D, Sato TN, Rabbany SY, Rafii S. Inductive angiocrine signals from sinusoidal endothelium are required for liver regeneration. *Nature* 2010;**468**:310–5
- Chen Y, Pu Q, Ma Y, Zhang H, Ye T, Zhao C, Huang X, Ren Y, Qiao L, Liu HM, Esmo CT, Ding BS, Cao Z. Aging reprograms the hematopoietic-vascular niche to impede regeneration and promote fibrosis. *Cell Metab* 2021;**33**:395–410
- Qing J, Ren Y, Zhang Y, Yan M, Zhang H, Wu D, Ma Y, Chen Y, Huang X, Wu Q, Mazhar M, Wang L, Liu J, Ding BS, Cao Z. Dopamine receptor D2 antagonism normalizes profibrotic macrophage-endothelial crosstalk in non-alcoholic steatohepatitis. *J Hepatol* 2022;**76**:394–406
- Wang L, Zhang Y, Ren Y, Yang X, Ben H, Zhao F, Yang S, Wang L, Qing J. Pharmacological targeting of cGAS/STING-YAP axis suppresses pathological angiogenesis and ameliorates organ fibrosis. *Eur J Pharmacol* 2022;**932**:175241
- Ren Y, Zhang Y, Wang L, He F, Yan M, Liu X, Ou Y, Wu Q, Bi T, Wang S, Liu J, Ding BS, Wang L, Qing J. Selective targeting of vascular endothelial YAP activity blocks EndMT and ameliorates unilateral ureteral obstruction-induced kidney fibrosis. *ACS Pharmacol Transl Sci* 2021;**4**:1066–74
- Chen L, Zhou T, White T, O'Brien A, Chakraborty S, Liangpunsakul S, Yang Z, Kennedy L, Saxena R, Wu C, Meng F, Huang Q, Francis H, Alpini G, Glaser S. The apelin-apelin receptor axis triggers cholangiocyte proliferation and liver fibrosis during mouse models of cholestasis. *Hepatology* 2021;**73**:2411–28
- Ferjancic S, Gil-Bernabe AM, Hill SA, Allen PD, Richardson P, Sparey T, Savory E, McGuffog J, Muschel RJ. VCAM-1 and VAP-1 recruit myeloid cells that promote pulmonary metastasis in mice. *Blood* 2013;**121**:3289–97
- Coll M, Ariño S, Martínez-Sánchez C, Garcia-Pras E, Gallego J, Moles A, Aguilar-Bravo B, Blaya D, Vallverdú J, Rubio-Tomás T, Lozano JJ, Pose E, Graupera I, Fernández-Vidal A, Pol A, Bataller R, Geng JG, Ginès P, Fernandez M, Sancho-Bru P. Ductular reaction promotes intrahepatic angiogenesis through Slit2-Roundabout 1 signaling. *Hepatology* 2022;**75**:353–68
- Sorajja P, Cable DG, Hamner CE, Schaff HV. Hirudin (desulfated, 54-65) contracts canine coronary arteries: extracellular calcium influx mediates hirudin-induced contractions. *J Surg Res* 2004;**121**:38–41
- Lovisa S, Fletcher-Sananikone E, Sugimoto H, Hensel J, Lahiri S, Hertig A, Taduri G, Lawson E, Dewar R, Revuelta I, Kato N, Wu CJ, Bassett RL, Jr, Putluri N, Zeisberg M, Zeisberg EM, LeBleu VS, Kalluri R. Endothelial-to-mesenchymal transition compromises vascular integrity to induce Myc-mediated metabolic reprogramming in kidney fibrosis. *Sci Signal* 2020;**13**:eaaz2597
- Haase VH. Mechanisms of hypoxia responses in renal tissue. *J Am Soc Nephrol* 2013;**24**:537–41
- Schuliga M, Grainge C, Westall G, Knight D. The fibrogenic actions of the coagulant and plasminogen activation systems in pulmonary fibrosis. *Int J Biochem Cell Biol* 2018;**97**:108–17
- Coughlin SR. Thrombin signalling and protease-activated receptors. *Nature* 2000;**407**:258–64
- Fiorucci S, Antonelli E, Distrutti E, Severino B, Fiorentina R, Baldoni M, Caliendo G, Santagada V, Morelli A, Cirino G. PAR1 antagonism protects against experimental liver fibrosis. Role of proteinase receptors in stellate cell activation. *Hepatology* 2004;**39**:365–75

31. Rullier A, Gillibert-Duplantier J, Costet P, Cubel G, Haurie V, Petibois C, Taras D, Dugot-Senant N, Deleris G, Bioulac-Sage P, Rosenbaum J. Protease-activated receptor 1 knockout reduces experimentally induced liver fibrosis. *Am J Physiol Gastrointest Liver Physiol* 2008;**294**:G226–35
32. Knight V, Tchongue J, Lourensz D, Tipping P, Sievert W. Protease-activated receptor 2 promotes experimental liver fibrosis in mice and activates human hepatic stellate cells. *Hepatology* 2012;**55**:879–87
33. Shearer AM, Rana R, Austin K, Baleja JD, Nguyen N, Bohm A, Covic L, Kuliopulos A. Targeting liver fibrosis with a cell-penetrating protease-activated receptor-2 (PAR2) pepducin. *J Biol Chem* 2016;**291**:23188–98
34. Joshi N, Kopec AK, O'Brien KM, Towery KL, Cline-Fedewa H, Williams KJ, Copple BL, Flick MJ, Luyendyk JP. Coagulation-driven platelet activation reduces cholestatic liver injury and fibrosis in mice. *J Thromb Haemost* 2015;**13**:57–71
35. Moya IM, Halder G. Hippo-YAP/TAZ signalling in organ regeneration and regenerative medicine. *Nat Rev Mol Cell Biol* 2019;**20**:211–26
36. Russell JO, Camargo FD. Hippo signalling in the liver: role in development, regeneration and disease. *Nat Rev Gastroenterol Hepatol* 2022;**19**:297–312
37. Kim J, Kim YH, Kim J, Park DY, Bae H, Lee DH, Kim KH, Hong SP, Jang SP, Kubota Y, Kwon YG, Lim DS, Koh GY. YAP/TAZ regulates sprouting angiogenesis and vascular barrier maturation. *J Clin Invest* 2017;**127**:3441–61
38. Mo JS, Yu FX, Gong R, Brown JH, Guan KL. Regulation of the Hippo-YAP pathway by protease-activated receptors (PARs). *Genes Dev* 2012;**26**:2138–43
39. Yu FX, Zhao B, Panupinthu N, Jewell JL, Lian I, Wang LH, Zhao J, Yuan H, Tumaneng K, Li H, Fu XD, Mills GB, Guan KL. Regulation of the Hippo-YAP pathway by G-protein-coupled receptor signaling. *Cell* 2012;**150**:780–91

(Received February 12, 2023, Accepted May 8, 2023)